Available online at www.sciencedirect.com

ScienceDirect

Current Opinion in Structural Biology

# Validating maps from single particle electron cryomicroscopy

Peter B Rosenthal[1] and John L Rubinstein[2,3,4]

Progress in single particle cryo-EM, most recently due to the introduction of direct detector devices, has made the high-resolution structure determination of biological assemblies smaller than 500 kDa more routine, but has also increased attention on the need for tools to demonstrate the validity of single particle maps. Although map validation is a continuing subject of research, some consensus has been reached on procedures that reduce model bias and over-fitting during map refinement as well as specific tests that demonstrate map validity. Tilt-pair analysis may be used as a method for demonstrating the consistency at low resolution of a map with image data. For higher-resolution maps, new procedures for more robust resolution assessment and for validating the refinement of atomic coordinate models into single particle maps have been developed.

**Addresses**
[1] Francis Crick Institute, Mill Hill Laboratory, London NW7 1AA, United Kingdom
[2] Molecular Structure and Function Program, The Hospital for Sick Children Research Institute, Toronto, Ontario M5G 1X8, Canada
[3] Department of Biochemistry, The University of Toronto, Toronto, Ontario M5S 1A8, Canada
[4] Department of Medical Biophysics, The University of Toronto, Toronto, Ontario M5G 1L7, Canada

Corresponding authors: Rosenthal, Peter B (peter.rosenthal@crick.ac.uk) and Rubinstein, John L (john.rubinstein@utoronto.ca)

**Current Opinion in Structural Biology** 2015, **34**:135–144

This review comes from a themed issue on **Biophysical and molecular biological methods**

Edited by **Ben Schuler** and **Janet L Smith**

For a complete overview see the Issue and the Editorial

**http://dx.doi.org/10.1016/j.sbi.2015.07.002**



## Introduction

Recent developments in both experimental and computational aspects of single particle electron cryomicroscopy (cryo-EM) have now fulfilled predictions that the method can be used for atomic resolution structure determination of protein and nucleic acid assemblies [1] by aligning and averaging images of non-crystalline single particles. Iterative refinement is typically used to bring a low-resolution starting map into higher resolution agreement with structural signal in the images (see Box 1). However, model-based assignment of particle orientations in low signal-to-noise ratio, low-dose images can be incorrect when map projections match the wrong features in an image or when they match noise. The persistence of an incorrect map or map features during refinement, referred to as model bias, is a real danger. For example, a crystal structure or homology model used as an initial reference during iterative refinement may yield a final map that shows high-resolution features such as α-helices and amino acid side-chains, but in fact only contains information present in the initial reference structure and not in the images [2••,3–5]. A related problem, termed over-refinement or over-fitting, occurs when the map matches signal in the images at low resolution, but at high resolution predominantly matches noise [6••,7,8]. The result of this over-fitting is the build-up of spurious noise features in the map that are reinforced during iterative refinement. Over-refined maps can possess features that resemble side-chain densities but in incorrect locations [9••].

At a similar stage in the development of X-ray crystallography, the problem of over-fitting of models during refinement was addressed by excluding a small fraction of reflection data ('free set') from the data used in refinement ('working set') for cross-validation. The 'Rwork', the residual error between the working set and reflections calculated from the model, can be driven to arbitrarily low values by including more refinement parameters, even when the model poorly matches the data, but decrease of the 'Rfree', the residual error between the free set and reflections calculated from the model, indicates true improvement in the model [10]. In recent years, progress has been made in single particle refinement schemes, including the use of maximum likelihood strategies that are less sensitive to model bias and over-fitting than earlier approaches [4,11–13]. In addition, specific validation tools have been developed and the importance of applying and reporting them during publication and database deposition has been agreed upon [14••]. Below we describe essential principles to ensure that single particle maps agree with data at low resolution and that the resolution of the structure determination is correctly assessed, particularly at high resolution. We emphasize specific tests that demonstrate the validity of a map without the requirement for independent re-determination of the map from raw data. We also describe similar principles and tests that may be applied to validating atomic models built into single particle maps.

## Is a map correct at low resolution?

An incorrect starting map may persist during refinement using existing tools, and therefore, validation tests should

**Box 1**

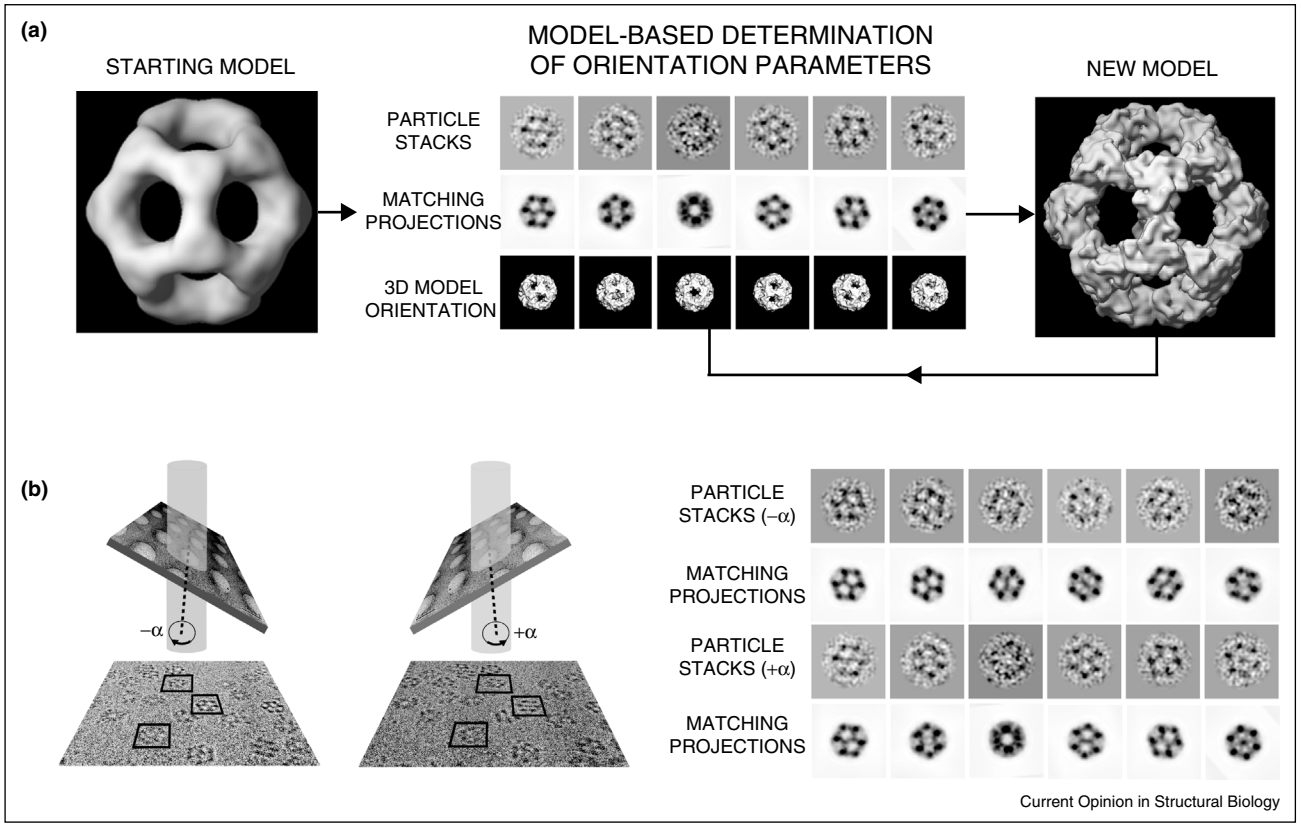


Model-based determination of orientation parameters from single particle images and tilt-pairs. (a) Projections of a low-resolution starting model are matched for agreement with a stack of particle images. Each image is thus assigned orientation parameters corresponding to the 3D model orientation that matches the image. In an iterative refinement scheme, a new model is computed from the images and the improved model is used to determine more accurate orientation parameters. (b) Images of a single field of particles are recorded at two angles ($-\alpha$ and $+\alpha$) of the microscope goniometer and are called a tilt-pair. A 3D map is used to determine orientation parameters for both particle stacks by projection matching. Figure based on data described in Ref. [23].

be applied from the very beginning of any structure determination. Because images containing only noise will align to the map during refinement, it is essential to demonstrate that individual particles of the reported size and shape are actually present and visible in images. Representative high contrast images may be obtained by employing a large objective lens defocus and sufficient electron exposure [2••]. Identification and selection of particle images in micrographs by cross-correlation with a template may select pure noise images [4,5,15]. In this case, subsequent image processing may be biased by the template. Consequently, the safeguard of visual examination of the micrographs and an initial round of manual particle picking by the investigator should always be employed.

Following particle selection, the next image processing steps are the alignment, classification and averaging of images of particles in similar orientations to produce high signal-to-noise views of the particle (class averages). The individual particle images that comprise the class should resemble the class average; this may be used as a criterion to select good particle images [16]. Subsequently, these class averages may be assigned orientations to calculate an initial map or they may serve as an intermediate stage in iterative map refinement. Reference-free procedures [3,17] that are less susceptible to noise matching a template, such as alignment of particles to a rotationally averaged sum of particle images or maximum likelihood strategies, should be used to calculate the first class averages. Similarly, projections of the 3D structure should agree with both class averages and raw images. Class averages that do not represent projections of the structure can arise when different views of a particle are inappropriately averaged or when noise in an image aligns to a 2D template. When particles adopt random orientations in an ice film, pairs of class averages that are mirror images of each other give support to those class averages being true 'views' of a macromolecular assembly [18].

Furthermore, 3D structure determination with isotropic resolution requires a wide distribution of particle views, although there are a number of ways in which an adequate distribution may be obtained [19]. The distribution of Euler angles assigned to particle images should be reported. Some map calculation algorithms can produce artefacts if specific particle orientations are over-represented [20]. Point symmetry determines which views should be averaged, the search range used to determine particle orientations, and the number of particle images needed to achieve a given resolution. Compelling evidence for views showing symmetry consistent with the point symmetry of a particle [21,22] should be obtained before that point symmetry is applied to the map. Proof of the symmetry ultimately requires validation of the map by a number of other tests, such as those described below.

A low-resolution map may have approximate agreement with images or class averages and still be incorrect. A more stringent criterion for a correct map is the simultaneous agreement of a map with image data recorded at two angles of the microscope goniometer. This agreement demonstrates the consistency of the map with structural features of the particle, which change predictably with tilt angle, showing that orientations are correctly assigned and that the map is not merely matching noise. The tilt-pair test is a simple procedure for cross-validation of orientation determination requiring a 3D map and a small representative sample of the data in the form of two stacks of particle images (e.g. 100 particles) from the same field of particles recorded at two different rotation angles of the microscope goniometer [23]. Tilt-pair analysis is now implemented in several image processing packages and as a web service ([24•], http://www.ebi.ac.uk/pdbe/emdb/validation/tiltpair/). This test can help detect the worst type of error in which a map is completely incorrect even at low resolution.

The tilt-pair test shows that the orientations assigned to the particles in the images agree with the known tilt angle and axis of the experiment. Plotting the tilt axis and tilt angle for each particle pair in a dataset, calculated from assigned orientations, and with a specification of the particle symmetry, yields a tilt-pair parameter plot (TPPP) [23,25••] (Figure 1a). A slightly different form of analysis, the tilt-pair phase residual plot, is shown in Figure 1b. The difference between the score for the map of correct hand compared to one of opposite hand (free-hand test) is a measure of the success in absolute hand determination, an important measure of the information content of a map [23,24•]. Both types of tilt-pair plots may be applied to the optimization of particle orientation determination such as the choice of data resolution range used for orientation determination. The width of the clusters on the TPPP is a measure of accuracy in orientation determination, which is greater for molecules of larger molecular weight. The tilt angle of the experiment should be chosen to be sufficiently large to distinguish clusters of points around the applied tilt angle from clusters around the origin, which may occur when the map does not match the image data. The question of when a TPPP validates a map or when it shows the map to be incorrect has been discussed by several investigators. A simple majority criterion has been proposed [25••] where 60% of particle tilt-pair parameters should be clustered around the known tilt angle and tilt axis. Otherwise, the reasons for the lack of agreement should be assessed by inspection of the tilt-pair data for processing errors or specimen heterogeneity. The significance of the tilt pair experiment may also be assessed against the expected result for random orientations by the tilt-pair alignment test [26••] (Figure 1c,d). More recently the clustering of the TPPP has been described by the concentration parameter ($\kappa$) of the Fisher distribution [27•]. A wide distribution of views should be used in the tilt-pair test. Selection of a subset of tilt-pair data that validates the map is an unfair application of the test and one that distorts its measure of orientational accuracy. Tilt-pair analysis has been used to assess particles covering a wide range of shapes and sizes embedded in ice. In negative stain, particle flattening may cause the tilt-pair test to have a minimum at a tilt angle less than the experimental angle.

A number of studies have argued for the validation of map refinement by demonstrating that multiple, independent refinements of different low-resolution starting maps all converge to the same structural features. Although this observation is circumstantial evidence that a map is correct, it does not exclude the possibility that there is a systematic bias toward an incorrect map (e.g. when refinement cannot distinguish orientations related by an approximate symmetry of a particle or is performed using a reference map of ill-defined hand, or when image datasets lack essential views), and independent validation criteria are still required to assess these results.

Cryo-EM maps and their interpretation can also be validated by biochemical experiments that localize a map feature by adding or removing a subunit, addition of covalently-linked polypeptide such as GFP [28] or MBP [29], antibodies [30–32], or protein (e.g. avidin [33]) or electron dense labels [34].

## Resolution assessment

A valid assessment of resolution indicates the accuracy with which a structural model may be built and adds confidence to functional interpretation. Validation of resolution assessment is essential to detect over-fitting and design refinement strategies that reduce spurious features at high resolution. The observed features of a map should be consistent with the resolution assessment (Figure 2). To visualize such features, maps must be

**Figure 1**

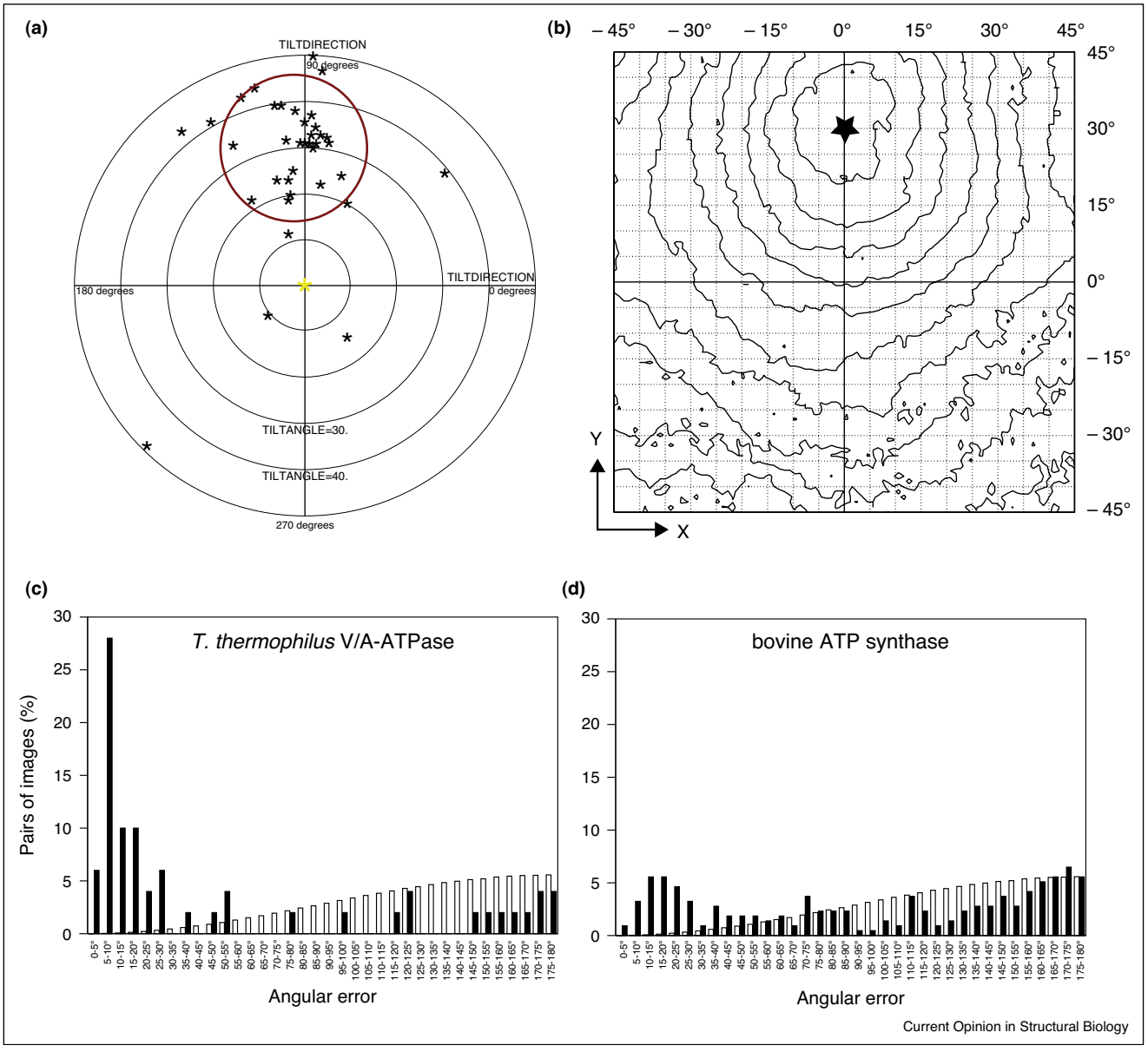


Map and orientation validation by tilt-pair analysis. **(a)** The *tilt-pair parameter plot* (TPPP) shows the in-plane tilt axis and angle for individual image pairs of *T. thermophilus* V/A-type ATPase recorded at −15° and +15° rotations of the goniometer. Particles for which orientations are correctly determined in both images cluster at the known tilt axis and angle of the experiment. Figure from Ref. [25••]. **(b)** The *tilt-pair phase residual plot* for the V/A-type ATPase shows the average phase residual score on the second image for each possible in-plane tilt axis and tilt angle applied to the orientation assigned to the first image. A minimum, marked with a star, occurs at (0,30), the known tilt transformation used in the experiment. The phase residual difference (freehand difference) between (0,30) and (0,−30) is 14.9°. Figure from Ref. [69]. **(c)** *Tilt-pair alignment test* shows that the angular errors for determination of the tilt transformation of each particle pair (black bars) from V/A-type ATPase particle orientations are much better than expected for random orientations (white bars). Data from Ref. [69]. **(d)** *Tilt-pair alignment test* shows that errors for calculated tilt transformations for bovine ATPase synthase (black bars) are worse than that for V/A-type, but still better than random (white bars). Data from Ref. [26••].

corrected for contrast loss at high resolution due to imperfections in images and computational errors in reconstruction described by an overall map temperature factor. Contrast may be restored by 'sharpening' with a negative temperature factor and figure-of-merit weighting [23,35,36]. The number of particle images required to reach a given resolution should sensibly reflect image quality and the known computational error in orientation

**Figure 2**

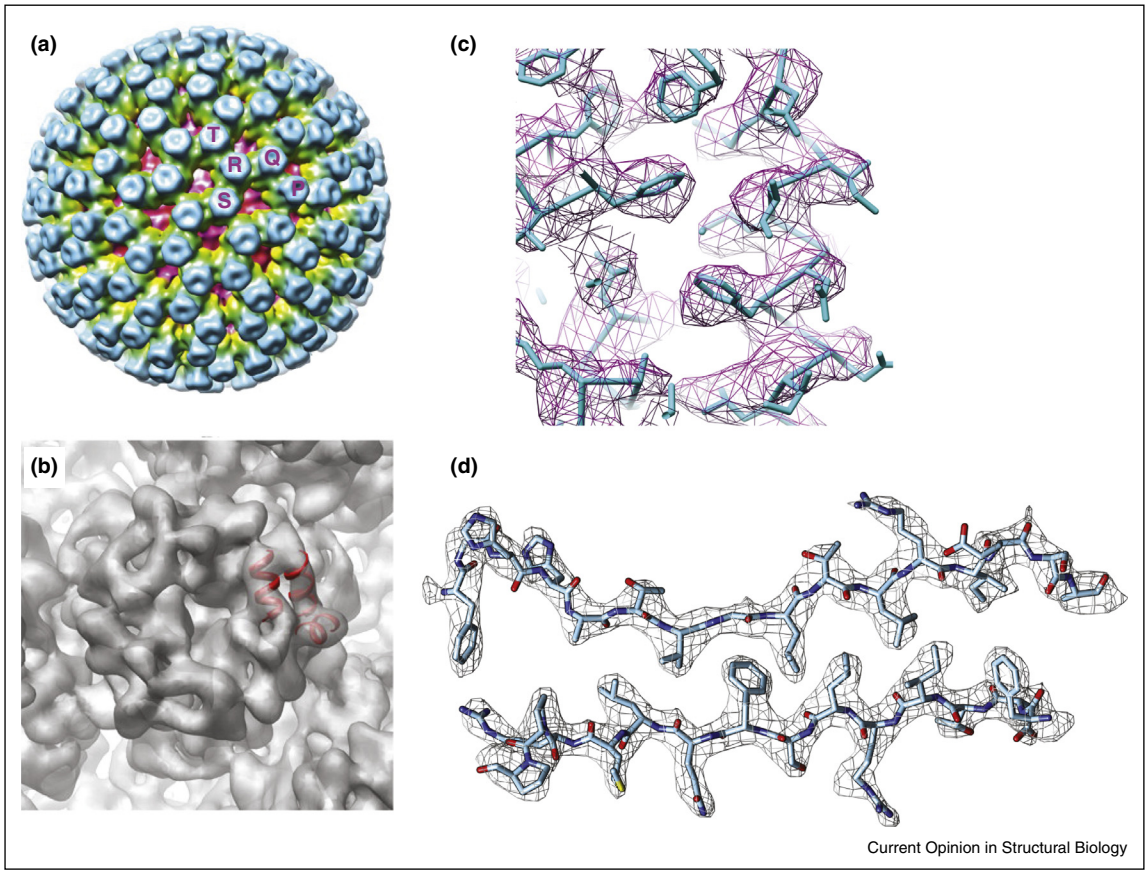


Map features depend on resolution. At resolutions worse than around 20 Å, just the overall envelope of a protein complex will be apparent. α-Helices are resolved past ~9–10 Å while distinguishing the strands of β-sheets requires resolutions better than 4.8 Å. At approximately 4 Å resolution some of the bulky side chains in amino acids can be detected. The resolution at which it becomes possible to build an all-atom model of a polypeptide is ~3.5 Å. Atomic model building becomes increasingly reliable with increasing resolution and is mostly robust around 2.5 Å resolution. **(a)** Rotavirus double-layered particle filtered to 20 Å, **(b)** filtered to 7 Å showing α-helices, **(c)** model built at 3.8 Å resolution. From Ref. [51]. Copyright 2008 The National Academy of Sciences. **(d)** Rotavirus DLP at 2.6 Å resolution (from EMDB-6272) [50], image kindly provided by the authors.

determination, the latter estimated by tilt-pair analysis [23,37].

The Fourier shell correlation (FSC) ([38–40], http://www.ebi.ac.uk/pdbe/emdb/validation/fsc/) is the most widely reported global measure of map resolution, although others have been proposed [41]. The FSC is the correlation between two 3D maps, each calculated from an independent half of the data (a 'half-map') as a function of resolution. The FSC is a measure of the signal-to-noise ratio of the map, which decreases with increasing resolution. The resolution of the map may be assigned when the FSC drops below a threshold (e.g. FSC = 0.143). However, the FSC curve may show features reflecting a number of potential problems [42] and should be plotted from the lowest resolution bin to the Nyquist frequency. It is also possible, due to limited accuracy in orientation determination or because some regions of the structure are less well-ordered than others, that there is not one single resolution that applies globally to the map. In this case, the FSC cut-off resolution is likely to represent the resolution of only part of the structure, especially if a large number of particle images have been used.

The FSC calculation assumes that the two half-maps are independent. Previously, it was deemed sufficient to separate the data used to calculate the FSC at the final iteration of map calculation. However, false or exaggerated resolution claims may result from the two halves of the dataset being over-fit to the same spurious noise features in a single reference map. It is now accepted that unless other safeguards are applied as described below, the two halves of the image dataset should be kept independent

during refinement and independent reference maps should be used [7,9••,14••]. In analogy with the Rfree, data could be omitted for cross-validation by leaving out a band of spatial frequencies [43]. More commonly, 'resolution limited' refinement is performed, where a maximum resolution cut-off for the data used in orientation determination during an iteration of refinement is chosen, and signal in the higher resolution 'free shells' is detected by correlation between the half-maps [9••,23,43]. The resolution limit for each cycle of refinement may be chosen in an automatic and unbiased way by using the FSC as a weight on the data during orientation determination [9••]. In practice, the highest-resolution data accessible by cryomicroscopy do not contribute to orientation determination and a lower-resolution limit may be chosen for particle refinement [23,25••]. Thus, resolution-limited refinement reduces the over-fitting but does not adversely affect the resolution of the final structure determination [9••]. In the past, when a single reference map and all spatial frequencies were used to align data for the two half-maps, an overly optimistic FSC curve was probably compensated by the more conservative FSC = 0.5 criterion rather than FSC = 0.143 [44].

In practice, any refinement, even where fully independently refined maps are compared, will introduce some amount of over-fitting. Chen *et al.* [6••] have proposed a test to detect over-fitting by making use of images where the phases of high-resolution structure factors are randomized or replaced entirely by structure factors from images of noise. Identical refinements using any protocol chosen by the investigator are then performed using the original images and the phase-randomized or noise-substituted images. The difference between the FSC from the original data (FSCt) and the FSC with high-resolution noise substitution or phase randomization (FSCn) represents the true high-resolution signal in the map (FSCtrue). (Figure 3a,b).

Molecular maps do not entirely fill the 3D volume of the box in which they are calculated and the region outside of the molecular envelope contains noise, which decreases the FSC and the reported resolution of the map. Typically a soft-edge mask is applied to limit the extent of the density. Unfortunately, use of the same mask in the two independent maps introduces artificial correlations between the maps leading to an over-estimate of resolution, particularly when the masks are so tight that they contact the map density. For this reason, authors should deposit an unmasked map as well as the masks applied to the final volume used to calculate the FSC [14••]. High-resolution noise substitution has also been applied to correct the FSC for the effect of the mask [6••] (Figure 3c).

Despite the value of global resolution measures, it is increasingly recognized that cryo-EM maps do not have uniform resolution throughout and possess regions of weaker density due to disorder and conformational and/or compositional heterogeneity. Inaccuracies in the determination of orientation parameters for particle images leads to the edges of maps being at lower resolution than the center where these inaccuracies have less of an effect [45••]. Several approaches have been proposed for examining local resolution [46]. The program ResMap searches for the smallest sinusoidal feature that can be detected above the noise at every point in a map, while accounting for the false discovery rate of the process [47]. Methods for analysing the variance in a structure determination provide information on the mobility of protein regions [48,49].

## Validating maps with atomic coordinate models and building valid models

Low-resolution map density may be validated by the agreement with the shape of an atomic model determined by X-ray crystallography, ideally with quantitative justification for a unique placement of the model as a rigid body within the map [14••]. The interpretation of the map with a model also chooses the absolute hand of the map. Alternatively, experimental determination of the absolute hand can be key in validating the fit of models to maps at low resolution. Where the structures of components undergo conformational changes in the context of a large assembly, they may be broken into several rigid bodies or flexibly fit (or morphed) into the map density. In this case, the density needs to be at sufficiently high resolution to justify the introduction of extra degrees of freedom to the model.

The rotavirus double-layered particle at 2.6 Å resolution [50,51] (Figure 2) is a spectacular example of the increasing number of high-resolution maps (5 maps better than 3 Å resolution [50,52–55] and >100 maps with better than 5 Å resolution in the Electron Microscopy Databank (EMDB)) that have made the building and assessment of atomic structure models an area of intense activity. Many tools developed for evaluating X-ray crystallographic models [56] may be applied in cryoEM [57–59]. The crystallographic phase problem results in initial maps with poor phases that improve during the course of refinement so that model building is an integral part of high-resolution map determination. In cryo-EM, the refinement of the experimental map is presently a separate step before model building. An atomic model may then be refined using a target that includes map amplitudes and phases as well as terms for model bonding and stereochemistry. A model may also be built for part of a map whose boundary is defined by a soft mask [60••]. EM maps are typically at lower resolution than X-ray diffraction data and new tools for building and refining into these lower resolution maps [60••,61–63] incorporate prior information or additional constraints that reduce the degrees of freedom and therefore over-fitting.

**Figure 3**

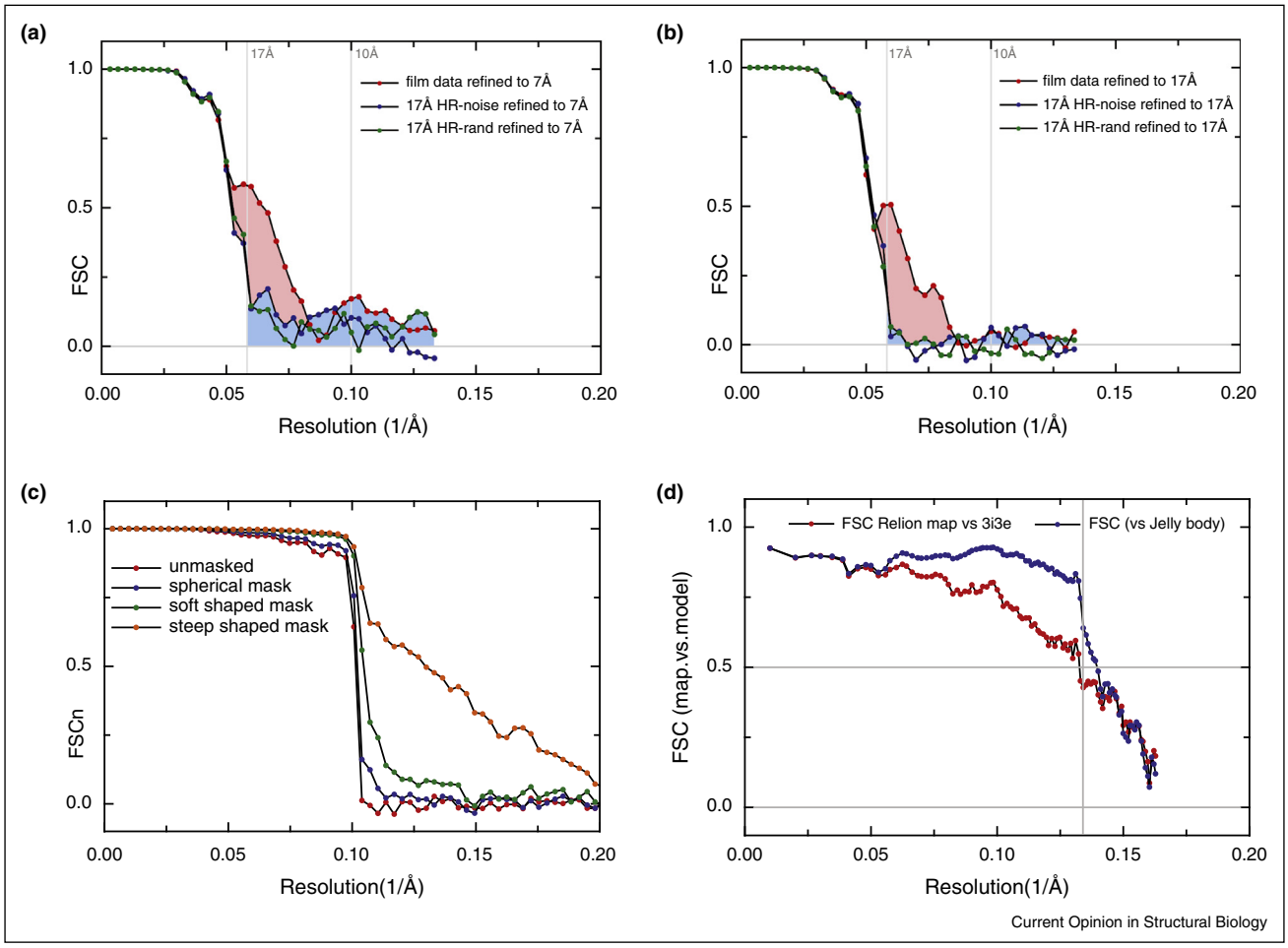


Resolution assessment by Fourier shell correlation (FSC) and its validation by the noise substitution test. **(a)** FSC between half-maps where particle orientation refinement uses image data to 7 Å resolution (red circle) or to 7 Å but where high resolution data beyond 17 Å has been substituted with data with randomized phases (HR-noise, green circle) or data from noise images (HR-noise, blue circle). Portion of FSC signal due to over-fitting is shown by the shaded blue region (FSCn), and the portion due to true structural signal is the shaded pink region (FSCtrue). **(b)** FSC curves as above but where particle orientation refinement has been limited to 17 Å resolution. The 'free shells' above 17 Å resolution show no over-fitting because they were not used in refinement. **(c)** FSCn between half-maps for noise-substituted data shows FSC artefacts that result from a tight mask. **(d)** FSC curve (red), also called Cref, between whole-map and coordinate model placed in the map by rigid body fitting crosses the 0.5 threshold at a point indicating 7.6 Å resolution. Flexible fitting of the model produces an overly optimistic FSC curve (blue). Panels are Figures 3a,b, 4b, and 5b of Ref. [6••].

As with X-ray models, measures of agreement between map and model include global statistics as well as local measures at specific main chain and amino acid side-chain positions. The FSC calculated between the model and the full map (Cref) is a global measure of the resolution of a map. For a perfect model and a map that does not have variable resolution in different regions the resolution at which Cref crosses 0.5 should be in agreement with the resolution assigned using the 0.143 threshold in the FSC between experimental half-maps [23]. With maps that have a variable resolution however, the map/model Cref plot may have Cref = 0.5 at a lower resolution than the half-map resolution at FSC = 0.143, implying that the model does not explain the map density quite as well as expected. The disagreement may be hidden (purposefully or unintentionally) by flexible fitting that allows too many degrees of freedom leading to an overly optimistic Cref as in Figure 3d [6••]. As with map refinement, high-resolution data beyond a cut-off may be excluded from model refinement with the high-resolution data range scored as free shells [64•]. The independently refined half-maps used to calculate the FSC have also been exploited for separate model refinement and cross-validation [60••,65•]. For example, in refinement of the

model for the 3.3 Å mitochondrial ribosome, the FSCwork between model and one half-map measured in 'free shells' at high resolution was compared with the FSCtest in the second half-map in 'free shells' of the same resolution range [60••,66,67].

## Conclusions and remaining problems

Structure determination by cryo-EM of single particles will continue to improve and will be extended to more challenging lower molecular weight and heterogeneous specimens. New, robust validation tools will need to accompany this development. High-resolution map features such as helices and side-chains are strong evidence of a valid structure determination. However, because of the danger of model bias, it must be clear that these features were not introduced from an external source during particle picking, 2D alignment, or 3D alignment, such as by aligning particle images with another EM map or map derived from a coordinate model. We therefore recommend performing as many tests as possible to communicate the validity of a map. Furthermore, validation tools may be applied to optimizing map calculation or for testing new computational procedures. For example, tilt-pair analysis tests the validity of a model at low-resolution but also demonstrates accurate orientation determination, which is a condition for high-resolution structure determination from modest numbers of particle images.

Heterogeneous particles raise several new problems in cryo-EM for which new validation tools may be required. High-resolution maps may be calculated from a small subset of the data (e.g. ~5%) [68]. From a validation standpoint, such a map may be correct but not represent the entire population of particles. Procedures to validate small differences in maps at high resolution will be an important development. As with macromolecular crystallography, public repositories such as the EMDB (www.emdatabank.org) will play an increasingly important role in providing standardized validation tools and validation reports that will be available while downloading maps and models. Computational tools, however, do not replace rigor at the biochemistry, specimen preparation, and image acquisition stages of the experiment: there will always be circumstances under which even the most robust tools can be misled.

## Conflict of interest statement

Nothing declared.

## Acknowledgements

P.B.R. is supported by the Francis Crick Institute which receives its core funding from Cancer Research UK, the UK Medical Research Council (program code U117581334), and the Wellcome Trust. J.L.R. is supported by operating grant MOP81294 from the Canadian Institutes of Health Research, discovery grant 401724-12 from the Natural Sciences and Engineering Research Council, and the Canada Research Chairs program. We thank Richard Henderson for comments on the manuscript.

## References and recommended reading

Papers of particular interest, published within the period of review, have been highlighted as:

- • of special interest
- •• of outstanding interest

1. Henderson R: **The potential and limitations of neutrons, electrons and X-rays for atomic-resolution microscopy of unstained biological molecules**. *Quart Rev Biophys* 1995, **28**:171-193.

2. •• Henderson R: **Avoiding the pitfalls of single particle cryo-electron microscopy: Einstein from noise**. *Proc Natl Acad Sci U S A* 2013, **110**:18037-18041.
Perspective on problems in single particle microscopy related to model bias, and recommendations on strategies and validation tools to avoid incorrect structures or exaggerated resolution claims.

3. Penczek P, Radermacher M, Frank J: **Three-dimensional reconstruction of single particles embedded in ice**. *Ultramicroscopy* 1992, **40**:33-53.

4. Sigworth FJ: **A maximum-likelihood approach to single-particle image refinement**. *J Struct Biol* 1998, **122**:328-339.

5. van Heel M: **Finding trimeric HIV-1 envelope glycoproteins in random noise**. *Proc Natl Acad Sci U S A* 2013, **110**:E4175-E4177.

6. •• Chen S, McMullan G, Faruqi AR, Murshudov GN, Short JM, Scheres SH, Henderson R: **High-resolution noise substitution to measure overfitting and validate resolution in 3D structure determination by single particle electron cryomicroscopy**. *Ultramicroscopy* 2013, **135**:24-35.
Test to demonstrate whether the calculated Fourier shell correlation (FSC) is an accurate assessment of structural signal at high resolution and determines portion of FSC signal due to over-fitting.

7. Grigorieff N: **Resolution measurement in structures derived from single particles**. *Acta Crystallogr D Biol Crystallogr* 2000, **56**:1270-1277.

8. Stewart A, Grigorieff N: **Noise bias in the refinement of structures derived from single particles**. *Ultramicroscopy* 2004, **102**:67-84.

9. •• Scheres SH, Chen S: **Prevention of overfitting in cryo-EM structure determination**. *Nat Methods* 2012, **9**:853-854.
Demonstration that using FSC weighting to perform frequency limited refinement of independent half-maps reduces over-fitting without reducing alignment accuracy and final map resolution.

10. Brunger AT: **Free R value: a novel statistical quantity for assessing the accuracy of crystal structures**. *Nature* 1992, **355**:472-475.

11. Lyumkis D, Brilot AF, Theobald DL, Grigorieff N: **Likelihood-based classification of cryo-EM images using FREALIGN**. *J Struct Biol* 2013, **183**:377-388.

12. Scheres SH: **RELION: implementation of a Bayesian approach to cryo-EM structure determination**. *J Struct Biol* 2012, **180**:519-530.

13. Scheres SH, Carazo JM: **Introducing robustness to maximum-likelihood refinement of electron-microscopy data**. *Acta Crystallogr D Biol Crystallogr* 2009, **65**:672-678.

14. •• Henderson R, Sali A, Baker ML, Carragher B, Devkota B, Downing KH, Egelman EH, Feng Z, Frank J, Grigorieff N *et al.*: **Outcome of the first electron microscopy validation task force meeting**. *Structure* 2012, **20**:205-214.
Review of the inaugural meeting of the Electron Microscopy Validation Task Force organized by the Electron Microscopy Databank (www.emdatabank.org). Reports consensus on map and model validation and database deposition.

15. Shaikh TR, Trujillo R, LeBarron JS, Baxter WT, Frank J: **Particle-verification for single-particle, reference-based reconstruction using multivariate data analysis and classification**. *J Struct Biol* 2008, **164**:41-48.

16. Yang Z, Fang J, Chittuluru J, Asturias FJ, Penczek PA: **Iterative stable alignment and clustering of 2D transmission electron microscope images**. *Structure* 2012, **20**:237-247.

17. Schatz M, van Heel M: **Invariant classification of molecular views in electron micrographs**. *Ultramicroscopy* 1990, **32**:255-264.

18. Rubinstein JL, Walker JE, Henderson R: **Structure of the mitochondrial ATP synthase by electron cryomicroscopy**. *EMBO J* 2003, **22**:6182-6192.

19. Baker LA, Rubinstein JL: **Angle determination for side views in single particle electron microscopy**. *J Struct Biol* 2008, **162**:260-270.

20. Sorzano CO, Marabini R, Boisset N, Rietzel E, Schroder R, Herman GT, Carazo JM: **The effect of overabundant projection directions on 3D reconstruction algorithms**. *J Struct Biol* 2001, **133**:108-118.

21. Crowther RA, Amos LA: **Harmonic analysis of electron microscope images with rotational symmetry**. *J Mol Biol* 1971, **60**:123-130.

22. Dube P, Tavares P, Lurz R, van HM: **The portal protein of bacteriophage SPP1: a DNA pump with 13-fold symmetry**. *EMBO J* 1993, **12**:1303-1309.

23. Rosenthal PB, Henderson R: **Optimal determination of particle orientation, absolute hand, and contrast loss in single-particle electron cryomicroscopy**. *J Mol Biol* 2003, **333**:721-745.

24. • Wasilewski S, Rosenthal PB: **Web server for tilt-pair validation of single particle maps from electron cryomicroscopy**. *J Struct Biol* 2014, **186**:122-131.
Web-based tilt-pair server now available at European Bioinformatics Institute (http://www.ebi.ac.uk/pdbe/emdb/validation/tiltpair/). Paper describes additional examples and procedures for using tilt-pair residual plots.

25. •• Henderson R, Chen S, Chen JZ, Grigorieff N, Passmore LA, Ciccarelli L, Rubinstein JL, Crowther RA, Stewart PL, Rosenthal PB: **Tilt-pair analysis of images from a range of different specimens in single-particle electron cryomicroscopy**. *J Mol Biol* 2011, **413**:1028-1046.
Applies tilt-pair parameter plots to a range of specimens of different molecular weight, shows the difference in orientation accuracy as a function of molecular weight, and relates these to the computational temperature factor describing contrast loss.

26. •• Baker LA, Watt IN, Runswick MJ, Walker JE, Rubinstein JL: **Arrangement of subunits in intact mammalian mitochondrial ATP synthase determined by cryo-EM**. *Proc Natl Acad Sci U S A* 2012, **109**:11675-11680.
Methods include quantification of accuracy in tilt pair tests through comparison of error distributions with that for random orientations.

27. • Russo CJ, Passmore LA: **Robust evaluation of 3D electron cryomicroscopy data using tilt-pairs**. *J Struct Biol* 2014, **187**:112-118.
Statistical analysis of tilt-pair parameter plots describing a concentration parameter $\kappa$ on the Fischer distribution.

28. Schreiber A, Stengel F, Zhang Z, Enchev RI, Kong EH, Morris EP, Robinson CV, da Fonseca PC, Barford D: **Structural basis for the subunit assembly of the anaphase-promoting complex**. *Nature* 2011, **470**:227-232.

29. Chen Z, Speck C, Wendel P, Tang C, Stillman B, Li H: **The architecture of the DNA replication origin recognition complex in *Saccharomyces cerevisiae***. *Proc Natl Acad Sci U S A* 2008, **105**:10326-10331.

30. Kim J, Wu S, Tomasiak TM, Mergel C, Winter MB, Stiller SB, Robles-Colmanares Y, Stroud RM, Tampe R, Craik CS *et al.*: **Subnanometre-resolution electron cryomicroscopy structure of a heterodimeric ABC exporter**. *Nature* 2015, **517**:396-400.

31. Smith TJ, Olson NH, Cheng RH, Liu H, Chase ES, Lee WM, Leippe DM, Mosser AG, Rueckert RR, Baker TS: **Structure of human rhinovirus complexed with Fab fragments from a neutralizing antibody**. *J Virol* 1993, **67**:1148-1158.

32. Vinothkumar KR, McMullan G, Henderson R: **Molecular mechanism of antibody-mediated activation of β-galactosidase**. *Structure* 2014, **22**:621-627.

33. Rubinstein J, Walker J: **ATP synthase from *Saccharomyces cerevisiae*: location of the OSCP subunit in the peripheral stalk region**. *J Mol Biol* 2002, **321**:613-619.

34. Al-Bassam J, Ozer RS, Safer D, Halpain S, Milligan RA: **MAP2 and tau bind longitudinally along the outer ridges of microtubule protofilaments**. *J Cell Biol* 2002, **157**:1187-1196.

35. Bottcher B, Wynne SA, Crowther RA: **Determination of the fold of the core protein of hepatitis B virus by electron cryomicroscopy**. *Nature* 1997, **386**:88-91.

36. Fernandez JJ, Luque D, Caston JR, Carrascosa JL: **Sharpening high resolution information in single particle electron cryomicroscopy**. *J Struct Biol* 2008, **164**:170-175.

37. Stagg SM, Noble AJ, Spilman M, Chapman MS: **ResLog plots as an empirical metric of the quality of cryo-EM reconstructions**. *J Struct Biol* 2014, **185**:418-426.

38. Saxton WO, Baumeister W: **The correlation averaging of a regularly arranged bacterial cell envelope protein**. *J Microsc* 1982, **127**:127-138.

39. van Heel M, Harauz G: **Resolution criteria for three dimensional reconstruction**. *Optik* 1986, **73**:119-122.

40. van Heel M, Stoffler-Meilicke M: **Characteristic views of *E. coli* and *B. stearothermophilus* 30S ribosomal subunits in the electron microscope**. *EMBO J* 1985, **4**:2389-2395.

41. Sousa D, Grigorieff N: **Ab initio resolution measurement for single particle structures**. *J Struct Biol* 2007, **157**:201-210.

42. Penczek PA: **Resolution measures in molecular electron microscopy**. *Methods Enzymol* 2010, **482**:73-100.

43. Shaikh TR, Hegerl R, Frank J: **An approach to examining model dependence in EM reconstructions using cross-validation**. *J Struct Biol* 2003, **142**:301-310.

44. Grigorieff N, Harrison SC: **Near-atomic resolution reconstructions of icosahedral viruses from electron cryo-microscopy**. *Curr Opin Struct Biol* 2011, **21**:265-273.

45. •• Kishchenko GP, Leith A: **Spherical deconvolution improves quality of single particle reconstruction**. *J Struct Biol* 2014, **187**:84-92.
Reports computational sharpening procedure reducing blur at high radius associated with particle mis-orientation

46. Cardone G, Heymann JB, Steven AC: **One number does not fit all: mapping local variations in resolution in cryo-EM reconstructions**. *J Struct Biol* 2013, **184**:226-236.

47. Kucukelbir A, Sigworth FJ, Tagare HD: **Quantifying the local resolution of cryo-EM density maps**. *Nat Methods* 2014, **11**:63-65.

48. Spahn CM, Penczek PA: **Exploring conformational modes of macromolecular assemblies by multiparticle cryo-EM**. *Curr Opin Struct Biol* 2009, **19**:623-631.

49. Zhang W, Kimmel M, Spahn CM, Penczek PA: **Heterogeneity of large macromolecular complexes revealed by 3D cryo-EM variance analysis**. *Structure* 2008, **16**:1770-1776.

50. Grant T, Grigorieff N: **Measuring the optimal exposure for single particle cryo-EM using a 2.6 Å reconstruction of rotavirus VP6**. *Elife* 2015:4.

51. Zhang X, Settembre E, Xu C, Dormitzer PR, Bellamy R, Harrison SC, Grigorieff N: **Near-atomic resolution using electron cryomicroscopy and single-particle reconstruction**. *Proc Natl Acad Sci U S A* 2008, **105**:1867-1872.

52. Bartesaghi A, Merk A, Banerjee S, Matthies D, Wu X, Milne JL, Subramaniam S: **2.2 Å resolution cryo-EM structure of beta-galactosidase in complex with a cell-permeant inhibitor**. *Science* 2015, **348**:1147-1151.

53. Campbell MG, Veesler D, Cheng A, Potter CS, Carragher B: **2.8 Å resolution reconstruction of the *Thermoplasma acidophilum* 20S proteasome using cryo-electron microscopy**. *Elife* 2015:4.

54. Fischer N, Neumann P, Konevega AL, Bock LV, Ficner R, Rodnina MV, Stark H: **Structure of the *E. coli* ribosome-EF-Tu complex at <3 Å resolution by Cs-corrected cryo-EM**. *Nature* 2015, **520**:567-570.

55. Jiang J, Pentelute BL, Collier RJ, Zhou ZH: **Atomic structure of anthrax protective antigen pore elucidates toxin translocation**. *Nature* 2015, **521**:545-549.

56. Read RJ, Adams PD, Arendall WB 3rd, Brunger AT, Emsley P, Joosten RP, Kleywegt GJ, Krissinel EB, Lutteke T, Otwinowski Z *et al.*: **A new generation of crystallographic validation tools for the protein data bank**. *Structure* 2011, **19**:1395-1412.

57. Emsley P, Cowtan K: **Coot: model-building tools for molecular graphics**. *Acta Crystallogr D Biol Crystallogr* 2004, **60**:2126-2132.

58. Murshudov GN, Skubak P, Lebedev AA, Pannu NS, Steiner RA, Nicholls RA, Winn MD, Long F, Vagin AA: **REFMAC5 for the refinement of macromolecular crystal structures**. *Acta Crystallogr D Biol Crystallogr* 2011, **67**:355-367.

59. Winn MD, Ballard CC, Cowtan KD, Dodson EJ, Emsley P, Evans PR, Keegan RM, Krissinel EB, Leslie AG, McCoy A *et al.*: **Overview of the CCP4 suite and current developments**. *Acta Crystallogr D Biol Crystallogr* 2011, **67**:235-242.

60. •• Brown A, Long F, Nicholls RA, Toots J, Emsley P, Murshudov G: **Tools for macromolecular model building and refinement into electron cryo-microscopy reconstructions**. *Acta Crystallogr D Biol Crystallogr* 2015, **71**:136-153.

Comprehensive discussion of model building and refinement into cryo-EM maps including cross-validation. Uses FSCwork in one-half map and FSCtest in second half-map with a further restriction to free-shells at high resolution.

61. DiMaio F, Tyka MD, Baker ML, Chiu W, Baker D: **Refinement of protein structures into low-resolution density maps using rosetta**. *J Mol Biol* 2009, **392**:181-190.

62. Headd JJ, Echols N, Afonine PV, Grosse-Kunstleve RW, Chen VB, Moriarty NW, Richardson DC, Richardson JS, Adams PD: **Use of knowledge-based restraints in phenix.refine to improve macromolecular refinement at low resolution**. *Acta Crystallogr D Biol Crystallogr* 2012, **68**:381-390.

63. Nicholls RA, Long F, Murshudov GN: **Low-resolution refinement tools in REFMAC5**. *Acta Crystallogr D Biol Crystallogr* 2012, **68**:404-417.

64. • Falkner B, Schroder GF: **Cross-validation in cryo-EM-based structural modeling**. *Proc Natl Acad Sci U S A* 2013, **110**:8930-8935 *Natl Acad Sci U S A*, 110, 2013, 8930–8935.

Cross-validation of atomic model refinement employing free shells at high resolution.

65. • DiMaio F, Zhang J, Chiu W, Baker D: **Cryo-EM model validation using independent map reconstructions**. *Protein Sci* 2013, **22**:865-868.

Cross-validation of model refinement by building a coordinate model into one half-map and monitoring the Fourier shell correlation (FSC) on second half-map.

66. Amunts A, Brown A, Bai XC, Llacer JL, Hussain T, Emsley P, Long F, Murshudov G, Scheres SH, Ramakrishnan V: **Structure of the yeast mitochondrial large ribosomal subunit**. *Science* 2014, **343**:1485-1489.

67. Brown A, Amunts A, Bai XC, Sugimoto Y, Edwards PC, Murshudov G, Scheres SH, Ramakrishnan V: **Structure of the large ribosomal subunit from human mitochondria**. *Science* 2014, **346**:718-722.

68. Fernandez IS, Bai XC, Hussain T, Kelley AC, Lorsch JR, Ramakrishnan V, Scheres SH: **Molecular architecture of a eukaryotic translational initiation complex**. *Science* 2013, **342**:1240585.

69. Lau WC, Rubinstein JL: **Structure of intact *Thermus thermophilus* V-ATPase by cryo-EM reveals organization of the membrane-bound V(O) motor**. *Proc Natl Acad Sci U S A* 2010, **107**:1367-1372.